# Renormalization of the phonon spectrum in semiconducting single-walled carbon nanotubes studied by Raman spectroscopy

Anindya Das and A. K. Sood*
*Department of Physics, Indian Institute of Science, Bangalore 560012, India*
(Received 19 February 2009; revised manuscript received 3 May 2009; published 23 June 2009)

*In situ* Raman experiments together with transport measurements have been carried out in single-walled carbon nanotubes as a function of electrochemical top gate voltage ($V_g$). We have used the green laser ($E_L$ =2.41 eV), where the semiconducting nanotubes of diameter ~1.4 nm are in resonance condition. In semiconducting nanotubes, the $G^-$- and $G^+$-mode frequencies increase by ~10 $cm^{-1}$ for hole doping, the frequency shift of the $G^-$ mode is larger compared to the $G^+$ mode at the same gate voltage. However, for electron doping the shifts are much smaller: $G^-$ upshifts by only ~2 $cm^{-1}$ whereas the $G^+$ does not shift. The transport measurements are used to quantify the Fermi-energy shift ($E_F$) as a function of the gate voltage. The electron-hole asymmetry in $G^-$ and $G^+$ modes is quantitatively explained using nonadiabatic effects together with lattice relaxation contribution. The electron-phonon coupling matrix elements of transverse-optic ($G^-$) and longitudinal-optic ($G^+$) modes explain why the $G^-$ mode is more blueshifted compared to the $G^+$ mode at the same $V_g$. The $D$ and $2D$ bands have different doping dependence compared to the $G^+$ and $G^-$ bands. There is a large downshift in the frequency of the $2D$ band (~18 $cm^{-1}$) and $D$ (~10 $cm^{-1}$) band for electron doping, whereas the $2D$ band remains constant for the hole doping but $D$ upshifts by ~8 $cm^{-1}$. The doping dependence of the overtone of the $G$ bands ($2G$ bands) shows behavior similar to the dependence of the $G^+$ and $G^-$ bands.

DOI: 10.1103/PhysRevB.79.235429 PACS number(s): 73.63.−b, 81.05.Uw, 78.30.Na

## I. INTRODUCTION

Single-walled carbon nanotubes continue to attract a lot of attention in recent years from the fundamental physics as well as novel application points of view. The reduced dimensionality-induced confinement effects result in imparting metallic or semiconducting character[1,2] to the tubes. The gate tunability of the transport of semiconducting nanotubes results in a field-effect transistor device, a key component of applications in nanoelectronics[3] and sensors.[4] An understanding of interaction of optical phonons with the charge carriers quantified by electron-phonon coupling (EPC) is important to understand the electron-transport mechanisms in nanotubes. For example, the upper limit of high-field ballistic transport in nanotubes is governed by electron scattering by optical phonons giving rise to hot phonon generation.[5,6]

Raman spectroscopy has proved to be a powerful noninvasive and nondestructive tool to characterize the carbon nanotubes as well as to probe electron-phonon coupling in them.[7] The most interesting Raman features in single-walled carbon nanotubes (SWNTs) are the radial breathing mode (RBM ~100–300 $cm^{-1}$) and tangential modes (near ~1590 $cm^{-1}$). The former is often used to determine the diameter and chirality of a SWNT.[1,2] The other Raman features are $D$ band (~1340 $cm^{-1}$) and $2D$ band (~2680 $cm^{-1}$) which involve the phonons belonging to the transversal optical branch near the zone boundary ($K$ point), whose peak positions depend on the exciting laser energy ($E_L$) due to double-resonance Raman scattering.[8] In the literature, the $2D$ mode has also been denoted as $G'$ and $D^*$. In general, the resonance Raman spectra of the tangential modes in semiconducting nanotubes have five bands, the most intense being $G^+$(~1590 $cm^{-1}$) and $G^-$(~1565 $cm^{-1}$) assigned to longitudinal-optic (LO) (axial) and transverse-optic (TO) (circumferential) modes, respectively.[1,9,10] The assignment of these modes for metallic tubes is, however, different: $G^+$(~1580 $cm^{-1}$) is assigned to the TO (circumferential) whereas $G^-$ (a broad band at ~1540 $cm^{-1}$) is LO (axial).[7,9,10] In particular, the metallic tubes are characterized by a $G^-$ mode with a large linewidth (~60 $cm^{-1}$) as compared to a narrow linewidth (~10 $cm^{-1}$) in the semiconducting tubes.[7]

The $G$ band in Raman spectrum of graphene arises due to doubly degenerate $E_{2g}$ phonon at the Brillouin-zone center ($\Gamma$).[1,2] This double degenerate $E_{2g}$ phonon splits into $G^+$ and $G^-$ modes in nanotube as the $sp^2$ bonds of graphene are deformed by rolling it in a tube. Thus, the simple curvature effect reasonably explains the downshifted $G^-$ (TO) band in semiconducting tubes.[10] However, in metallic tubes, the large downshift and the large linewidth of the $G^-$ (LO) mode is due to the enhanced EPC (resulting from electron confinement in one dimension) between the LO phonon and the electron-hole excitations, which is termed as nonadiabatic Kohn anomaly.[7,9–12] It has been shown recently that due to the nonadiabatic effect, the $G^-$-peak position in metallic tubes[13–17] and the $G$-band position (~1582 $cm^{-1}$) in single[18–21] and bilayer[22–24] graphenes increase both for electron as well as hole doping, whereas the linewidths of these bands decrease for both types of doping.[13–17,19–24] In comparison to the metallic nanotubes, phonon renormalization in doped semiconducting nanotubes has not been fully studied experimentally. This has motivated us to undertake the present study, employing resonant Raman scattering from top-gated electrochemically doped semiconducting tubes.

We will briefly summarize the existing results on electrochemical doping of semiconducting tubes. Kavan *et al.*[25] showed that the frequency of the $G^+$ mode remains constant for the gate voltage ($V_g$) from −1.5 to +1 V. When $V_g$ is

 

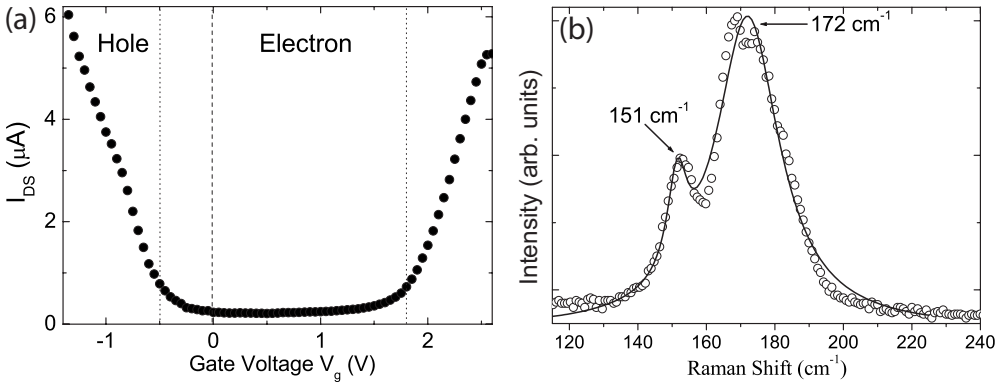


FIG. 1. (a) Drain-source current ($I_{DS}$) vs gate voltage ($V_g$). The vertical dotted lines correspond to the onset of currents for electron and hole dopings. The dashed vertical line is the charge neutrality point (CNP). (b) RBM of nanotube bundles at 2.41 eV showing peaks at 151 ($d$=1.6 nm) and 172 cm$^{-1}$ ($d$=1.4 nm).

increased beyond +1 V (hole doping), the frequency upshifts to a maximum of ~15 cm$^{-1}$ for $V_g$=+1.6 V. On electron doping, the frequency downshifts by ~3 cm$^{-1}$ at $V_g$=−1.8 V. Corio *et al.*[26,27] also showed a similar behavior of the $G^+$ mode in semiconducting tubes. However, Rafailov *et al.*[28,29] showed a linear shift in the $G^+$ mode at 1.3 cm$^{-1}$/V to higher (lower) frequencies on hole (electron) doping. The total shift was less than 3 cm$^{-1}$ for hole doping and 1 cm$^{-1}$ for electron doping. In all these studies the shift of the Fermi level in terms of applied $V_g$, a key parameter to quantitatively understand the results has not been reported. Further, the effect of doping on the $G^-$ mode is not experimentally determined, except in Ref. 29 where the upshift of the $G^-$(1.6 cm$^{-1}$/V) for hole doping is slightly higher as compared to the $G^+$(1.3 cm$^{-1}$/V). In our very recent experiments[13] on SWNT bundles using $E_L$=1.96 eV, the mode observed at ~1590 cm$^{-1}$ was attributed to the $G^+$ (LO) mode of semiconducting tubes which upshifted by ~6 cm$^{-1}$ for hole doping and only ~1 cm$^{-1}$ for the electron doping. Since the Raman band at ~1590 cm$^{-1}$ recorded with $E_L$=1.96 eV can also arise from metallic nanotubes,[15,30] the results were rather preliminary.

In this paper, we have carried out *in situ* Raman experiments together with transport measurement on SWNT bundles with green laser ($E_L$=2.41 eV), where only the semiconducting tubes are in resonance condition. The transport measurements help us to quantify the Fermi-level shift as a function of the gate voltage. The frequency shifts of the $G^+$ and $G^-$ modes in semiconducting tubes are measured as a function of Fermi energy for both electron and hole dopings and compared with the theoretical calculations in terms of nonadiabaic effects using time-dependent perturbation theory (TDPT), together with doping-induced lattice relaxation. We will also quantify the evolution of other high-energy modes $D$, $2D$, and $2G$ modes as a function of Fermi energy, where $2G$ is the overtone of the $G$ band.

## II. EXPERIMENTAL

As described earlier,[13] the ac dielectrophoresis[31] technique is used to align the nanotubes between two gold electrodes (separated by 15 μm), which act as source and drain. The Fermi energy is shifted by electrochemical top gating using solid polymer electrolyte consisting of $LiClO_4$ and polyethylene oxide in the ratio of 0.12:1,[32,33] where the gate voltage is applied by placing a platinum electrode in the polymer layer. As shown for the nanotubes and graphene,[13,19] the polymer electrolyte gives a more efficient way of doping the system up to a much higher doping level at comparatively smaller gate voltages $V_g$. This is because the nanometer thick Debye layer[19] gives a much higher gate capacitance as compared to the usual 300-nm-thick $SiO_2$ gate layer used in back gating field-effect transistors.[34] Raman spectra are measured with a WITEC confocal (X50 objective) spectrometer with 600 lines/mm grating, 514.5 nm excitation (2.41 eV) and very low power level (~1 mW) to avoid any heating effect. In a single Raman spectrum we capture the $G$, $D$, $2D$, and $2G$ Raman modes. Figure 1(b) shows the Raman spectrum of the RBM modes of the nanotubes using the green laser of $E_L$=2.41 eV. It shows two Raman bands at 151 cm$^{-1}$ and 172 cm$^{-1}$. Using the relation[35] between the frequency of the RBM $\omega_{RBM}$ and diameter $d$ of the tube $\omega_{RBM}(\text{cm}^{-1})=\frac{219}{d(nm)}+15$, we estimate that the sample has tubes of average diameters 1.4 and 1.6 nm. The laser at 2.41 eV is in resonance with $E_{33}^S$ of nanotubes of $d$=1.4 nm and $E_{44}^S$ of nanotubes of $d$=1.6 nm.[36] Since the Raman intensity corresponding to the RBM of 1.4 nm average diameter tubes is much higher than the intensity of the RBM Raman mode of 1.6 nm tubes, the dominant contribution to the high-energy Raman modes comes from the 1.4 nm semiconducting tubes.

## III. RESULTS

Figure 1(a) shows the conductivity of the nanotubes as a function of gate voltage, keeping source-drain voltage fixed at 50 mV. Here we see the ambipolar behavior in the conductivity plot of our nanotube-based field-effect transistor device. The off current is ~0.2 μA at $V_g$=0 V and current increases in either side from $V_g$=0 V. Therefore, there is no significant intrinsic doping in the sample. We see a sharp change in the conductivity at higher positive (electron doping) and negative (hole doping) gate voltages because of Van Hove singularities in the density of states (DOS) of the semi-

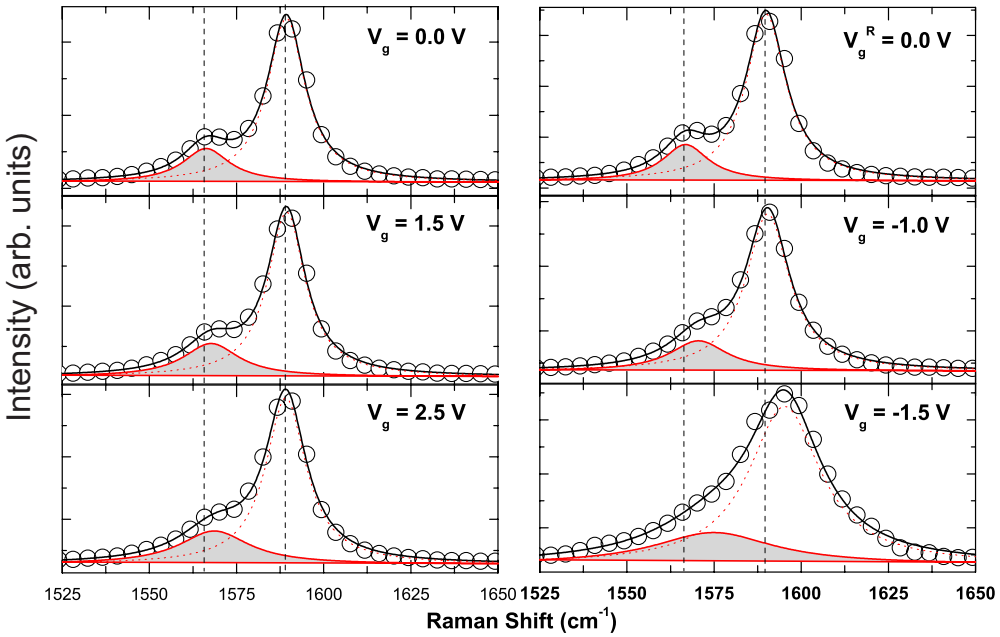


FIG. 2. (Color online) Tangential Raman modes of SWNTs recorded using an excitation energy of 2.41 eV at several gate voltage ($V_g$). The open circles show the raw Raman spectra and the lines are the fitted one. The shaded Raman spectra show the $G^-$ (TO) mode of the semiconducting nanotubes.

conducting nanotubes. Even though our sample contains metallic tubes due to large energy separation of $E_{11}^M \sim 1.8$ eV the change in conductivity due to gating is governed mainly by the semiconducting tubes. Among the semiconducting tubes, the 1.6 nm tubes will dominate the conductance as it has a smaller band gap ($E_{11}^S \sim 0.5$ eV) compared to the 1.4 nm tubes ($E_{11}^S \sim 0.6$ eV). It can be seen from Fig. 1(a) that there is large asymmetry in the onset of conduction for electron and hole doping. This arises due to large Schottky barrier for electron doping at the interface of gold electrodes and semiconducting nanotubes. This was already seen by Derycke *et al.*[37] The work functions of gold electrode and carbon nanotube are $\sim -5.1$ eV and $\sim -4.7$ eV, respectively. Therefore, for hole doping the separation between the Fermi energies of gold electrode and semiconducting nanotube will decrease which will reduce the Schottky barrier height. However, for electron doping the separation will increase leading to an enhanced Schottky barrier height.[38] Thus, for electron doping there will be a larger Schottky barrier as compared to the hole doping.

Figure 2 shows the typical $G$ band Raman spectra recorded at different gate voltages. A constant gate voltage is applied for 5 min to stabilize the $I_{DS}$ before the Raman spectrum is recorded for the next 30 s. Spectra are well fitted with two Lorentzians centered at $\sim 1565$ cm$^{-1}$($G^-$) and $\sim 1590$ cm$^{-1}$($G^+$). We have chosen to fit the spectra with two Lorentzians because the other three bands[2] in semiconducting tubes at $\sim 1525$, 1550, and 1610 cm$^{-1}$ are much weaker than the $G^+$ and $G^-$ modes, and hence cannot be followed as a function of gate voltages. The change in Raman frequency $[\Delta\omega = \omega(V_g) - \omega(V_g = 0)]$ and the full width at half maximum (FWHM) are plotted in Fig. 3 as a function of gate voltage. The frequency of the $G^-$ remains almost constant up to $V_g \sim -0.5$ V and then smoothly increases by $\sim 10$ cm$^{-1}$ for higher hole doping. For electron doping, the frequency of the $G^-$ mode remains almost constant up to $V_g \sim 2.8$ V and then increases only by $\sim 2$ cm$^{-1}$. Similarly, the $G^+$ peak remains constant up to $V_g \sim -0.8$ V and then starts increasing showing a upshift of $\sim 8$ cm$^{-1}$ for $V_g = -1.8$ V. However, there is almost no shift of $G^+$ peak for electron doping even at maximum $V_g$ of 3.5 V. Therefore, there is a large asymmetry in the frequency shift of $G^+$ and $G^-$ modes for the hole and electron dopings. We note that the frequency shift of the $G^-$ mode is slightly larger compared to

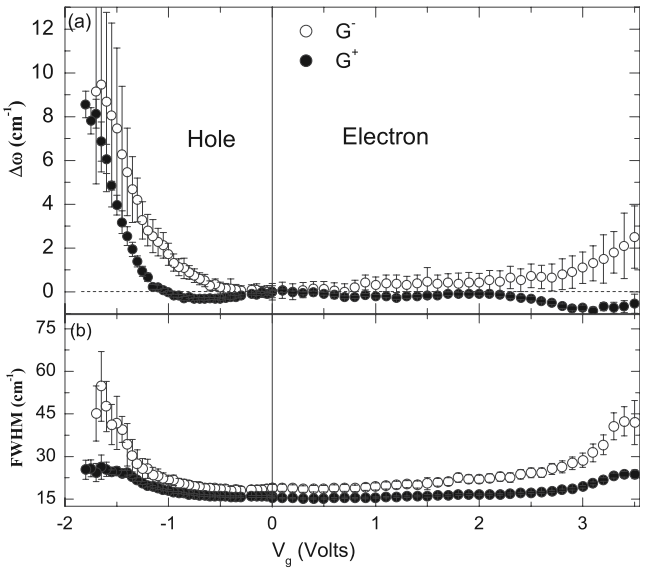


FIG. 3. (a) Position of $G^-$ (open circles) and $G^+$ (close circles) peaks as a function of gate voltages ($V_g$). (b) $V_g$-dependent FWHM of $G^-$ (open circles) and $G^+$ (close circles) modes in semiconducting tubes.

the $G^+$ mode at a same gate voltage ($V_g$). Figure 3(b) shows that the FWHM of $G^-$ and $G^+$ remains constant for $V_g$ from −1.0 to 3.0 V, increasing at higher gate voltages. Here, also the increase is higher for the $G^-$ mode as compared to the $G^+$ mode.

## IV. DISCUSSION

### A. Nonadiabatic correction

To explain these experimental trends, we consider the effects of doping on $G^-$ and $G^+$ modes. The main contribution comes from the nonadiabatic or "dynamic" effects due to electron-phonon coupling, denoted by $\Delta\omega^{\mathrm{dyn}}(E_F)=\omega^{\mathrm{dyn}}(E_F)-\omega^{\mathrm{dyn}}(E_F=0)$. The physics behind the dynamic effect is basically how the carriers screen the phonon vibrations. The carrier screening can be expressed in terms of phonon decay into interband electron-hole excitations, as shown in Fig. 4(a). Since, the lowest-energy gap (2Δ) between the first Van Hove singularities in valence and conduction bands, [$E_{11}^S$(~0.55 eV) of the semiconducting nanotubes] is much higher than the phonon energy $\hbar\omega_G$(~0.196 eV), therefore, the phonon can only decay into virtual electron-hole excitations. Now, as the Fermi energy enters in the conduction or valence band, some of virtual electron-hole excitations will be blocked because of Pauli exclusion principle, as shown schematically in Fig. 4(a), which will reduce the screening of phonons by the carriers, resulting in an upshift of the phonon frequency with respect to the undoped case. This effect will be symmetric for both the electron and hole dopings. The nonadiabatic effect calculated using TDPT is given for $q=0$ phonon as[11]

$$\Delta\omega^{\mathrm{dyn}}(E_F)=\mathrm{Re}\left[\frac{1}{\hbar}\int_{-\bar{k}}^{\bar{k}}\frac{A_0\hbar}{M\omega_0\pi^2 d}\times\lambda^2(k)\sum_{s\neq s'}\frac{\delta f(\epsilon_{sk})-\delta f(\epsilon_{s'k})}{\epsilon_{sk}-\epsilon_{s'k}+\hbar\omega_0+i\delta}dk\right] \quad (1)$$

where $\lambda(k)$ is the electron-phonon coupling constant of a semiconducting tube, $A_0=5.24$ Å$^2$ is the graphene unit-cell area, $M$ is the carbon atom mass, $d$ is the diameter of the semiconducting tube, $\delta f(\epsilon)=f(\epsilon)^{E_F}-f(\epsilon)^{E_F=0}$, and $f(\epsilon)=[\exp(\frac{\epsilon-E_F}{k_BT})+1]^{-1}$ is the Fermi-Dirac distribution.

$\delta$ accounts for the finite lifetime of the electronic states. $\hbar\omega_0$ is the phonon energy in undoped condition, $s,s'=\pm1$ label the conduction (+1) and valence (−1) bands, and $\epsilon_{sk}=s\sqrt{(\beta k)^2+(\Delta)^2}$ is the hyperbolic energy dispersion of carriers in semiconducting nanotube. The $\beta=\frac{\sqrt{3}}{2}\gamma_0 a$, where $\gamma_0$ is the nearest-neighbor tight-binding parameter, $a$(=2.49 Å) is the graphene lattice parameter, and Δ is the half of the band gap. The electron-phonon coupling constant of a semiconducting tube can be written as[11]

$$\lambda^2(k)=\Lambda^2\left(1\pm\frac{(\beta k)^2-\Delta^2}{(\beta k)^2+\Delta^2}\right), \quad (2)$$

where Λ is the electron-phonon coupling constant of graphene and ± sign correspond to LO ($G^+$) and TO ($G^-$) modes, respectively. Using Eq. (2), we have plotted the EPC

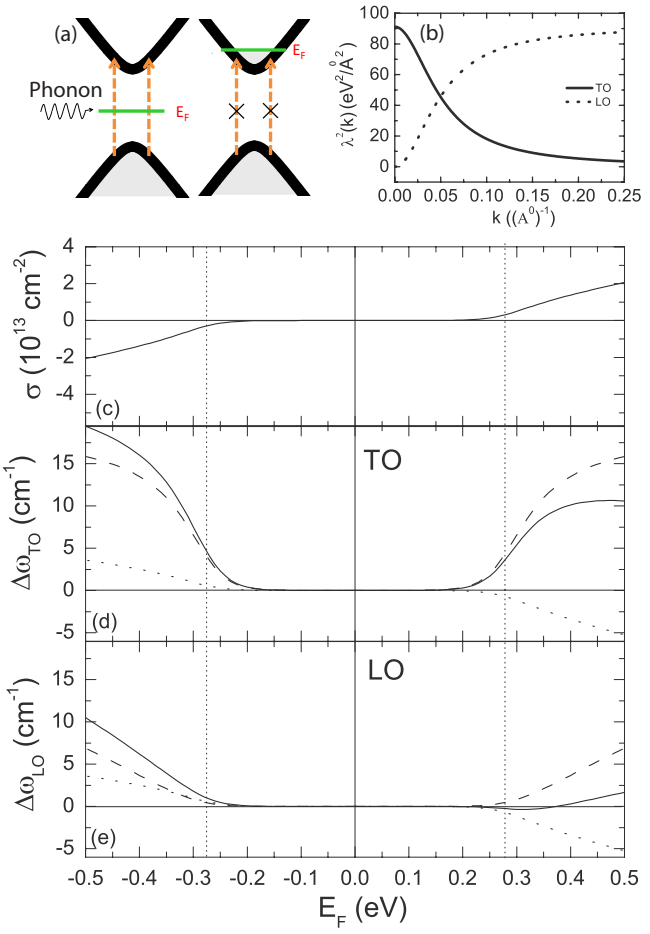


FIG. 4. (Color online) (a) Decay of phonon into interband electron-hole excitations when the Fermi energy ($E_F$) at CNP (left panel). Some of the electron-hole excitations are blocked due to Pauli exclusion principle when the $E_F$ enters in the conduction band (right panel). (b) EPC matrix element as a function of electronic wave vector ($k$) for LO (dotted line) and TO (solid line). (c) Theoretical charge doping in a semiconducting nanotube in terms of $10^{13}$/cm$^2$ (see the text) at 300 K. Dynamic effect (dashed line), lattice relaxation effect (dotted line), and total phonon renormalization (solid line) for (d) TO and (e) LO as a function of Fermi-energy shift. The dotted vertical lines are the position of the first Van Hove singularities.

($\lambda^2(k)$) as a function of $k$ in Fig. 4(b) using the values of the parameters of $\Lambda^2$ and $\beta$ given by density-functional calculations, $\Lambda^2=45.6$ (eV)$^2$/Å$^2$ and $\beta=5.52$ eV Å (Ref. 18). We have used $d=1.4$ nm and $\Delta=0.275$ eV ($E_{11}^S/2$ of 1.4 nm tube). The EPC matrix element for TO is maximum at $k=0$ and decreases with $k$, whereas for LO it is zero at $k=0$ and increases with $k$. As a result, the frequency shift of the TO mode ($G^-$) would be larger compared to the LO mode ($G^+$) when the Fermi-energy shift blocks the transitions near the band edge ($k=0$). Recently, it has been shown that the proper inclusion of nonlocal exchange-correlation[39] effect significantly renormalizes $\Lambda^2$ and it will be interesting to see how this inclusion will modify the electron-phonon coupling for the semiconducting nanotube.

In Figs. 4(d) and 4(e) we have plotted Eq. (1) for the TO ($G^-$) and LO ($G^+$) modes (dashed lines) as a function of

Fermi-energy shift at 300 K. We have seen that the theoretical curve is not sensitive to the value of $\delta$. The value of $\delta = 0.001$ eV was used. We have taken the limit $\bar{k} = 0.25$ Å$^{-1}$ such that $\epsilon(\bar{k}) \gg \Delta E_F$ (Fermi-energy shift). We should mention that the Fermi-energy shift in our experiment is $\sim 0.4$ eV which will result in blocking the electronic transitions up to $k \sim 0.05$ Å$^{-1}$. As seen in Figs. 4(d) and 4(e), the frequency shifts (dashed lines) of the TO ($G^-$) and LO ($G^+$) modes due to nonadiabatic effect are symmetric for both sides of doping and the frequency shift of the TO ($G^-$) mode is larger compared to the LO ($G^+$) mode.

### B. Lattice-relaxation effect

The nonadiabatic effect does not explain the large electron-hole asymmetry seen in $G^+$ and $G^-$ modes in Fig. 3(a). To explain this, we need to consider the effect of doping on the phonons due to the doping-induced change in the equilibrium lattice parameter, usually termed as static effect and denoted by $\Delta\omega^{\text{static}}$. There is no calculation available in literature on $\Delta\omega^{\text{static}}$ for the nanotubes. However, the bond-length change due to the doping has been calculated for a single-layer graphene using density functional theory and the change in $\Gamma$ phonon frequency ($G$ mode) with doping is fitted to an empirical relation[18]

$$\Delta\omega_G^{\text{static}}(\text{cm}^{-1}) = -2.13\sigma - 0.036\,0\sigma^2 - 0.003\,29\sigma^3 - 0.226|\sigma|^{3/2} \quad (3)$$

where $\sigma$ is the electron (hole) density in units of $10^{13}/\text{cm}^2$. The electron density ($n$) in a semiconducting tube is calculated as $n = \int_0^\infty D(\epsilon) f(\epsilon) d\epsilon$, where $D(\epsilon) = \frac{4\epsilon}{\pi\beta\sqrt{\epsilon^2 - \Delta^2}}$ is the electronic density of states and calculated from the hyperbolic energy dispersion. Now to calculate the phonon shift for the nanotube, we express $n$ in terms of $\sigma$ of graphene by simple dimensional analysis. The density in terms of carriers per unit circumferential area for the nanotube can be written as $\sigma = n/\pi d$. In Fig. 4(c) we have plotted the charge density in terms of $\sigma(10^{13}/\text{cm}^2)$ for semiconducting nanotube ($d = 1.4$ nm) at 300 K as a function of Fermi energy. Now, using Eq. (3), $\Delta\omega^{\text{static}}$ is plotted in Figs. 4(d) and 4(e) (dotted lines). Here, we have assumed that the lattice relaxation is same for the LO and the TO modes. We are aware of the fact that for the LO mode with vibration along the axis, our assumption may be a right description. However, due to the loss of planarity in the TO mode (circumferential), it may not be the complete description but may serve as a first step toward understanding our data.

The total phonon-frequency renormalization in a semiconducting nanotube can thus be written as

$$\Delta\omega = \Delta\omega^{\text{static}} + \Delta\omega^{\text{dyn}} \quad (4)$$

The solid lines in Figs. 4(d) and 4(e) show the total phonon renormalization using Eq. (4).

### C. Conversion of $V_g$ into $E_F$

To compare these theoretical trends with our experimental results (Fig. 3), it is necessary to convert gate voltage ($V_g$) into the Fermi-energy ($E_F$) shift. In general, the application of a gate voltage ($V_g$) creates an electrostatic potential difference $\phi$ between the nanotube and the gate electrode, and a Fermi-level ($E_F$) shifts as a result of the addition of charge carriers. Therefore, $V_g = \frac{E_F}{e} + \phi$. The $\phi$ and $E_F/e$ are determined by the geometrical capacitance ($C_g$) and the quantum capacitance ($C_Q$) of the nanotube, respectively. Now, the electrostatic potential $\phi = \frac{ne}{C_g}$, where $n$ is the carrier concentration which can be calculated using the relation $n = \int_0^{E_F} D(\epsilon) d\epsilon$ and given by

$$n = 0; \quad E_F < \Delta$$

$$= \frac{4}{\pi\beta}\sqrt{E_F^2 - \Delta^2}; \quad E_F \geq \Delta \quad (5)$$

Thus, for a semiconducting nanotube

$$V_g = \frac{E_F}{e}; \quad E_F < \Delta$$

$$= \frac{E_F}{e} + \frac{4e}{\pi\beta C_g}\sqrt{E_F^2 - \Delta^2}; \quad E_F \geq \Delta \quad (6)$$

Now, the $C_g$ is determined by the thickness of the Debye layer ($d_{\text{Debye}}$) for an electrochemical gating[13,19,22] and its value is reported to be few nanometers ($\sim 1$–$4$ nm).[32] For the case of nanotube, we can write $C_g = \frac{2\pi\epsilon\epsilon_0}{\ln(1 + \frac{2d_{\text{Debye}}}{d})}$ using cylindrical capacitor model. For $d_{\text{Debye}} = 2$ nm,[19] $\epsilon = 5$, and $d = 1.4$ nm we obtain $C_g = 2 \times 10^{-10}$ F/m. Therefore, using Eq. (6), one can convert the $V_g$ into $E_F$. It can be seen from Eq. (6) that when $E_F < \Delta$, there will be complete conversion of $V_g$ into $E_F$ with a proportionality factor $\alpha = 1 (E_F = \alpha e V_g)$. This can also be understood because $C_Q \propto \text{DOS}$ (Refs. 38 and 40) which is zero for $E_F < \Delta$ and hence $C_Q \ll C_g$. However, in real situations, there will be finite DOS near the charge neutrality point due to temperature and adsorbate-induced band-structure modifications as well as there will be a finite Schottky barrier at the nanotube-gold electrode interface. Thus the proportionality factor $\alpha$ will be less than 1 and Eq. (6) can rewritten as

$$V_g = \frac{E_F}{\alpha e}; \quad E_F < \Delta$$

$$= \frac{E_F}{\alpha e} + \frac{4e}{\pi\beta C_g}\sqrt{E_F^2 - \Delta^2}; \quad E_F \geq \Delta \quad (7)$$

The proportionality factor $\alpha$ is estimated from the onset of currents in the transport measurements. The onset of currents in Fig. 1(a), which are marked by vertical dotted lines at $V_g \sim -0.55$ V and $\sim 1.75$ V, correspond to the first Van Hove singularities at $-0.25$ eV and 0.25 eV in the valence band and conduction band, respectively. Thus, the proportionality factors estimated from the transport measurements are $\alpha_h \sim \frac{-0.25}{-0.55} = 0.45$ and $\alpha_e \sim \frac{0.25}{1.75} = 0.14$, and the different values of $\alpha$ can arise due to a larger Schottky barrier for electron doping as compared to hole doping. Using Eq. (7), Fig. 5 shows $\Delta\omega_{G^+}$ and $\Delta\omega_{G^-}$ as a function of Fermi energy. We

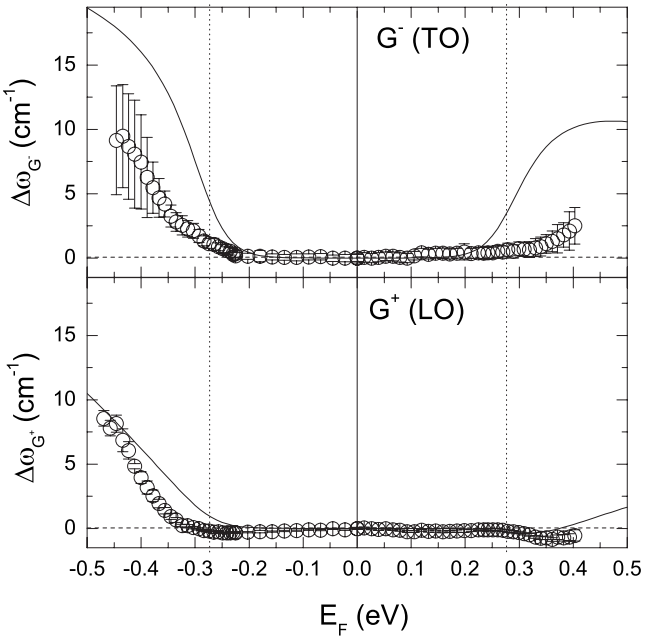


FIG. 5. Position of $G^-$ (TO) mode and $G^+$ (LO) mode of semiconducting nanotube as a function of Fermi-energy shift. Open circles are the experimental data and the solid lines are the theoretical predications combining the dynamic and the lattice-relaxation effect. The dotted vertical lines are the position of the first Van Hove singularities.

note that the agreement between experiments and theory is reasonable.

### D. Linewidths

As mentioned before, the $G^+$ and $G^-$ phonons ($\sim$0.196 eV) can only cause virtual electron-hole interband transitions. These excitations contribute only to the real part of phonon self-energy without affecting the imaginary part. Therefore, the FWHM should remain constant with Fermi-energy shift. This agrees with our experimental data [Fig. 2(b)] except at very high gate voltages. The increase in FWHM seen at high voltages can be due to inhomogeneous broadening. There can be screening of the electric field by the outer tubes in a nanotube bundle resulting in different $E_F$ shifts in different nanotubes. This may cause the increase in the FWHM at higher $V_g$ since the frequency position is sensitive to $E_F$.

## V. *D* AND 2*D* MODES

Now we will focus on the *D* mode and its overtone mode 2*D*, where both the modes correspond to the phonons belonging to the transversal-optical branch near the *K* point as explained by the double-resonance Raman process.[8] Before discussing our results, we will briefly summarize the available results on the *D* and 2*D* modes with electrochemical biasing. Using $E_L$=2.54 eV, Corio *et al.*[26,27] showed that the *D* and 2*D* modes do not shift up to $V_g$=1.2 V, then they upshift abruptly by $\sim$10 cm$^{-1}$ (*D* mode) and $\sim$18 cm$^{-1}$ (2*D* mode) at $V_g$=1.4 V (hole doping). Rafailov *et al.*[29] showed

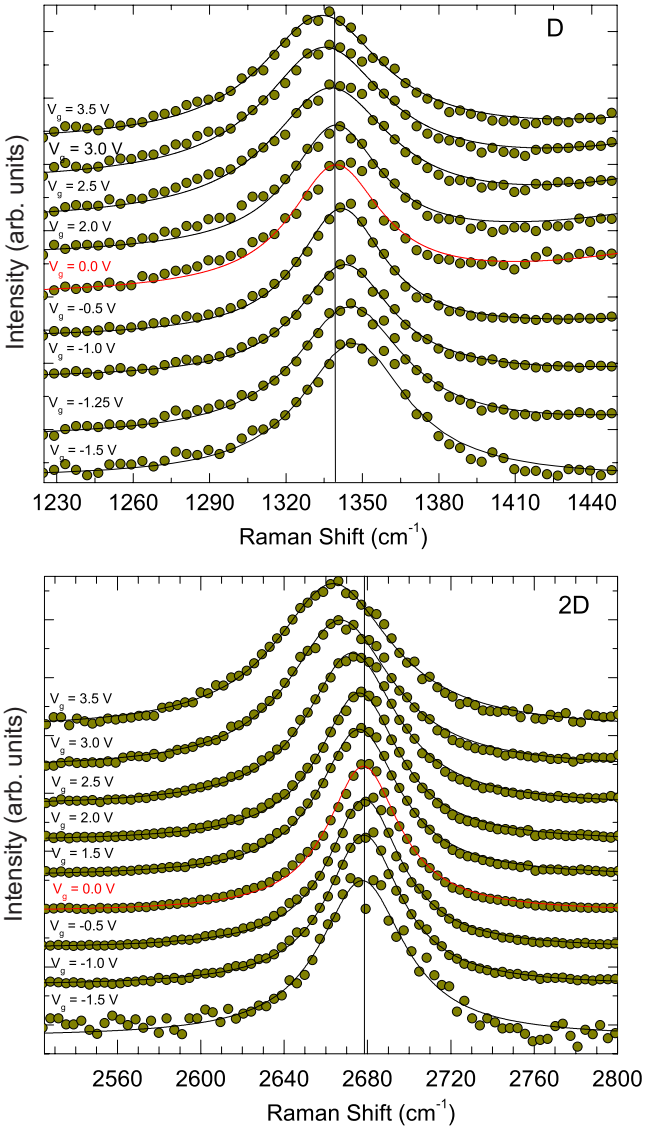


FIG. 6. (Color online) Raman spectra of *D* and 2*D* at several gate voltages ($V_g$). Filled circles are the raw data and solid lines are the fitted one. Red line (light gray) corresponds to the undoped case.

that the shift of the 2*D* mode depends on $E_L$. It upshifts by a very small amount of $\sim$2 cm$^{-1}$ at $V_g$=1 V (hole doping) with $E_L$=2.41 eV. However, it is $\sim$5 cm$^{-1}$ at $V_g$=1 V with $E_L$=1.96 eV. In all these experiments, there is no data on the electron doping. Also as mentioned before, the Fermi-energy shift has not been quantified.

Figure 6 shows the Raman spectra of the *D* and the 2*D* modes at several gate voltages. We have fitted the spectra with single Lorentzian (solid lines) and shown in Fig. 7. The frequency shift and linewidth are plotted in Fig. 8 as a function of $E_F$. The frequency of the 2*D* mode decreases with electron doping (downshifts by 15 cm$^{-1}$ at $E_F\sim$0.35 eV) but it remains almost constant for hole doping. The frequency softening of the 2*D* band with electron doping in semiconducting tube is very similar to that of single-layer graphene.[19] However, there is a large difference on the hole side; in a single-layer graphene, the frequency of the 2*D*

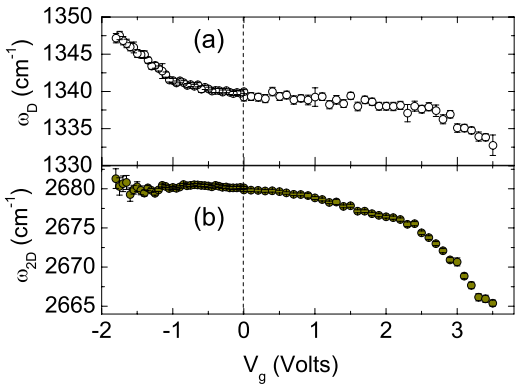


FIG. 7. (Color online) Frequency position of (a) $D$ and (b) $2D$ as a function of gate voltages.

band upshifts by a large amount whereas it is almost constant in semiconducting tubes. The most striking result is the evolution of the $D$ mode. As seen in Fig. 8(a), the $D$ mode downshifts by $\sim 7$ cm$^{-1}$ for electron doping, which is half of the downshift of the $2D$ mode, as expected. However, the situation on the hole side is totally surprising. The $D$ mode upshifts by $\sim 8$ cm$^{-1}$ with hole doping in contrast to no shift of the $2D$ mode. We have yet to understand this surprising result for which additional work may be required.

Figure 9(a) shows the area ratio of $D$ and $2D$ modes as a function of Fermi-energy shift. We should mention here that the intensity ratio has similar trend like the area ratio. Here, we have plotted the area ratio instead of intensity ratio as the linewidths (FWHM) vary significantly with Fermi-energy shift, as seen in Fig. 9(b). It can be seen from Fig. 9(a) that at higher electron and hole doping, the area of the $D$ band increases by almost ten times compared to the undoped case. Figures 9(b) and 9(c) plot the variation in the area ratios of

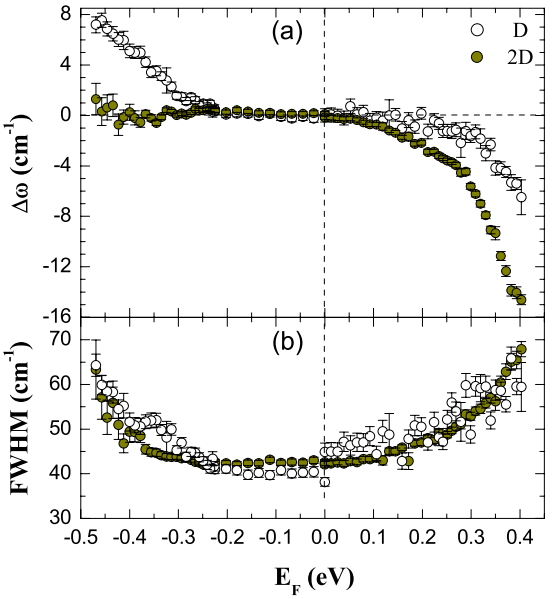


FIG. 8. (Color online) (a) Frequency shift of $D$ (open circles) and $2D$ (filled circles) as a function of Fermi energy. (b) FWHM of $D$ (open circles) and $2D$ (filled circles) as a function of Fermi energy.

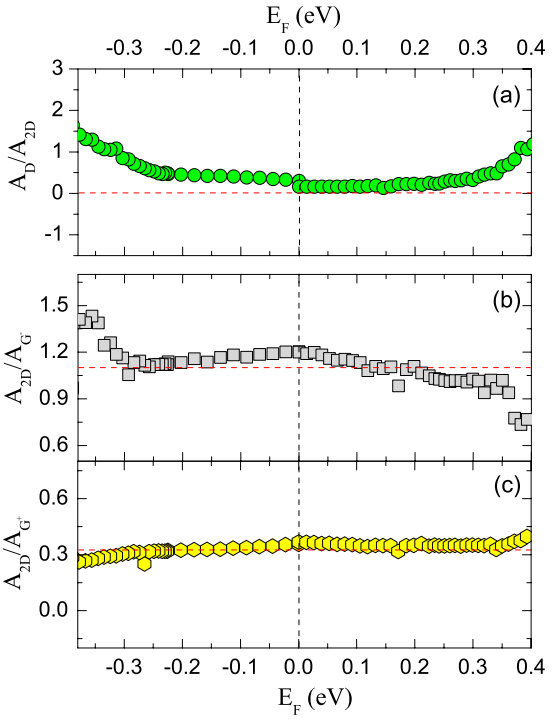


FIG. 9. (Color online) (a) Area ratio of $D$ and $2D$, (b) area ratio of $2D$ and $G^-$, and (c) area ratio of $2D$ and $G^+$ as a function of the Fermi-energy shift.

the $2D$ and $G^-$ mode ($A_{2D}/A_{G^-}$), and the $2D$ and $G^+$ mode ($A_{2D}/A_{G^+}$), respectively, as a function of the Fermi-energy shift. However, the intensity ratios ($I_{2D}/I_{G^-}$ and $I_{2D}/I_{G^+}$) also follow the similar trend like the area ratios. We note that unlike graphene,[19] $A_{2D}/A_G$ ratios do not vary much with doping, which suggests that the $A_{2D}/A_G$ ratios cannot be used to monitor the doping levels in the semiconducting tubes. This behavior is very similar to that of the bilayer graphene.[22] It will be interesting to study experimentally the dependence of $A_{2D}/A_G$ ratio as a function of the Fermi-energy shift in the metallic tubes.

## VI. OVERTONE OF THE $G$ MODE

Now we look at the overtone mode $2G$, which has not been studied before as a function of the Fermi-energy shift. Figure 10 shows the Raman spectra of the $2G$ band at several gate voltages. At $E_F=0$, the $2G^+$ is the most intense band at $\sim 3180$ cm$^{-1}$, the other two weaker bands being at $\sim 3155$ cm$^{-1}$ and $\sim 3220$ cm$^{-1}$. The band at 3155 cm$^{-1}$ is slightly higher than the overtone of the $G^-$ mode ($2 \times 1565$ cm$^{-1}$) and the band at 3220 cm$^{-1}$ is an overtone of a mode at 1610 cm$^{-1}$ seen in the Raman spectra of the nanotube. The Raman spectra are fitted with three Lorentzians; but at higher positive ($\approx 3$ V) and negative ($\approx -1.3$ V)$V_g$, we could not fit it and hence the frequency shift is being plotted in Fig. 11 from $E_F=-0.3$ eV($V_g=-1.3$ V) to 0.3 eV ($V_g=3$ V). Similar to the $G^+$ mode, $2G^+$ shifts only for the hole doping and there is almost no shift for the electron side. The shifts of the $2G^+$ and $2G^+$ for the hole side are almost double that of the $G^+$ and $G^-$ modes, respectively. The solid

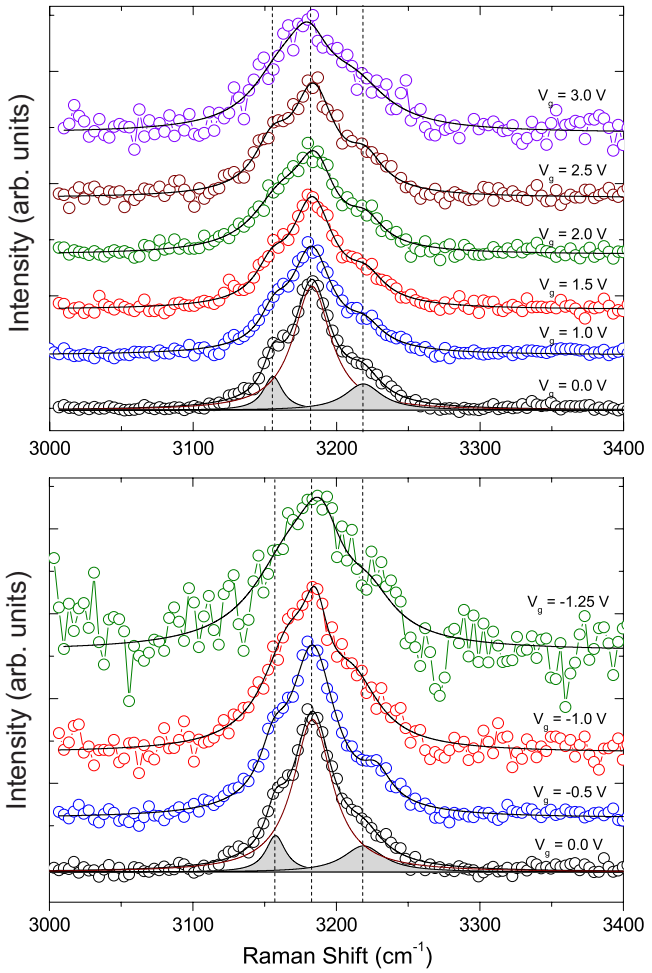


FIG. 10. (Color online) Raman spectra of $2G$ band at several gate voltages. Open circles with connecting lines are the raw data. Solid lines are the fitted one. The shaded regions correspond to the peaks at $\sim 3155$ cm$^{-1}$ and $\sim 3220$ cm$^{-1}$ at undoped case.

lines in Figs. 11(a) and 11(b) are plotted using Eq. (4) after multiplying by a factor of 2.

## VII. CONCLUSIONS

In summary, by combining transport and *in situ* Raman experiments with theoretical calculations, we have quantified the effect of doping on phonons in semiconducting nanotubes. The Raman measurements show that the $G$ and $2D$ bands have different doping dependences. The electron-hole asymmetry in the $G^+$ and $G^-$ modes is explained in terms of

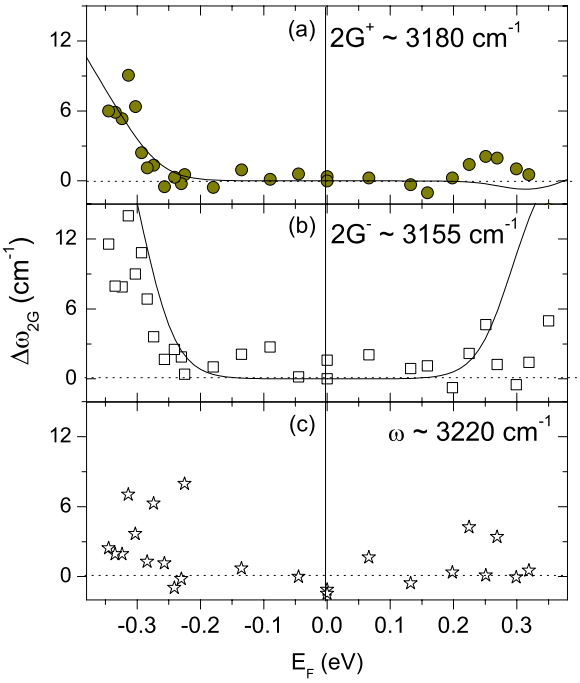


FIG. 11. (Color online) The position of (a) $2G^+(3180\ \text{cm}^{-1})$, (b) $2G^-(3155\ \text{cm}^{-1})$, and (c) $\omega \sim 3220\ \text{cm}^{-1}$ modes as a function of Fermi energy. The solid lines are the theoretical curves.

nonadiabatic effects together with the lattice-relaxation contribution. The dependence of the electron-phonon coupling matrix elements on wave vector $k$ explains why the $G^-$ mode is more blueshifted compared to the $G^+$ mode. The shift of the $2D$ band is very different as compared to the $G^+$ and $G^-$ modes: there is a redshift on electron doping but no shift on hole doping. We also presented the experimental data on the $D$ and the $2G$ bands as a function of the Fermi-energy shift. Our results on semiconducting nanotubes can help in providing an understanding of phonon renormalization due to doping and at the same time contribute to determine the amount and the type of doping level in semiconducting nanotube-based nanoelectronic devices. We hope that our experimental results will motivate the theoretical studies to quantitatively understand the doping dependence of the modes, in particular, the $2D$ band.

## ACKNOWLEDGMENTS

We thank C.N.R. Rao for nanotube samples and discussions. A.K.S. thanks the Department of Science and Technology, India, for financial assistance.

*asood@physics.iisc.ernet.in

[1] S. Reich, C. Thomsen, and J. Maultzsch, *Carbon Nanotubes: Basic Concepts and Physical Properties* (Wiley-VCH, New York, 2004).
[2] R. Saito, G. Dresselhaus, and M. S. Dresselhaus, *Physical Properties of Carbon Nanotubes* (Imperical College, London, 1998).
[3] S. Tans, A. Verschueren, and C. Dekker, Nature (London) **393**, 49 (1998).
[4] S. Ghosh, A. K. Sood, and N. Kumar, Science **299**, 1042 (2003).
[5] E. Pop, D. Mann, J. Cao, Q. Wang, K. Goodson, and H. J. Dai, Phys. Rev. Lett. **95**, 155505 (2005).
[6] M. Lazzeri, S. Piscanec, F. Mauri, A. C. Ferrari, and J. Robert-

son, Phys. Rev. Lett. **95**, 236802 (2005).
[7] M. Lazzeri, S. Piscanec, F. Mauri, A. C. Ferrari, and J. Robertson, Phys. Rev. B **73**, 155426 (2006).
[8] C. Thomsen and S. Reich, Phys. Rev. Lett. **85**, 5214 (2000).
[9] O. Dubay, G. Kresse, and H. Kuzmany, Phys. Rev. Lett. **88**, 235506 (2002).
[10] S. Piscanec, M. Lazzeri, J. Robertson, A. C. Ferrari, and F. Mauri, Phys. Rev. B **75**, 035427 (2007).
[11] N. Caudal, A. M. Saitta, M. Lazzeri, and F. Mauri, Phys. Rev. B **75**, 115423 (2007).
[12] S. Piscanec, M. Lazzeri, F. Mauri, A. C. Ferrari, and J. Robertson, Phys. Rev. Lett. **93**, 185503 (2004).
[13] A. Das, A. K. Sood, A. Govindaraj, A. M. Saitta, M. Lazzeri, F. Mauri, and C. N. R. Rao, Phys. Rev. Lett. **99**, 136803 (2007).
[14] H. Farhat, H. Son, G. G. Samsonidze, S. Reich, M. S. Dresselhaus, and J. Kong, Phys. Rev. Lett. **99**, 145506 (2007).
[15] Y. Wu, J. Maultzsch, E. Knoesel, B. Chandra, M. Huang, M. Y. Sfeir, L. E. Brus, J. Hone, and T. F. Heinz, Phys. Rev. Lett. **99**, 027402 (2007).
[16] K. T. Nguyen, A. Gaur, and M. Shim, Phys. Rev. Lett. **98**, 145504 (2007).
[17] J. C. Tsang, M. Freitag, V. Perebeinos, J. Liu, and P. Avouris, Nat. Nanotechnol. **2**, 725 (2007).
[18] M. Lazzeri and F. Mauri, Phys. Rev. Lett. **97**, 266407 (2006).
[19] A. Das, S. Pisana, B. Chakraborty, S. Piscanec, S. K. Saha, K. S. Novoselov, U. Waghmare, H. R. Krishnamurhthy, A. K. Geim, A. C. Ferrari, and A. K. Sood, Nat. Nanotechnol. **3**, 210 (2008).
[20] S. Pisana, M. Lazzeri, C. Casiraghi, K. Novoselov, A. K. Geim, A. C. Ferrari, and F. Mauri, Nature Mater. **6**, 198 (2007).
[21] J. Yan, Y. Zhang, P. Kim, and A. Pinczuk, Phys. Rev. Lett. **98**, 166802 (2007).
[22] A. Das, B. Chakraborty, S. Piscanec, S. Pisana, A. K. Sood, and A. C. Ferrari, Phys. Rev. B **79**, 155417 (2009).
[23] J. Yan, E. A. Henriksen, P. Kim, and A. Pinczuk, Phys. Rev. Lett. **101**, 136804 (2008).
[24] L. M. Malard, D. C. Elias, E. S. Alves, and M. A. Pimenta, Phys. Rev. Lett. **101**, 257401 (2008).
[25] L. Kavan, P. Rapta, L. Dunsch, M. J. Bronikowski, P. Willis, and R. E. Smalley, J. Phys. Chem. B **105**, 10764 (2001).
[26] P. Corio, P. S. Santos, V. W. Brar, G. G. Samsonidze, S. G. Chou, and M. S. Dresselhaus, Chem. Phys. Lett. **370**, 675 (2003).
[27] P. Corio, A. Jorio, N. Demir, and M. S. Dresselhaus, Chem. Phys. Lett. **392**, 396 (2004).
[28] M. Stoll, P. M. Rafailov, W. Frenzel, and C. Thomsen, Chem. Phys. Lett. **375**, 625 (2003).
[29] P. M. Rafailov, M. Stoll, and C. Thomsen, J. Phys. Chem. B **108**, 19241 (2004).
[30] M. Kalbac, L. Kavan, L. Dunsch, and M. S. Dresselhaus, Nano Lett. **8**, 1257 (2008).
[31] R. Krupke, F. Hennrich, H. V. Lohneysen, and M. M. Kappes, Science **301**, 344 (2003).
[32] C. Lu, Q. Fu, S. Huang, and J. Liu, Nano Lett. **4**, 623 (2004).
[33] G. P. Siddons, D. Merchin, J. H. Back, J. K. Jeong, and M. Shim, Nano Lett. **4**, 927 (2004).
[34] A. K. Geim and K. S. Novoselov, Nature Mater. **6**, 183 (2007).
[35] P. T. Araujo, S. K. Doorn, S. Kilina, S. Tretiak, E. Einarsson, S. Maruyama, H. Chacham, M. A. Pimenta, and A. Jorio, Phys. Rev. Lett. **98**, 067401 (2007).
[36] T. Michel, M. Paillet, J. C. Meyer, V. N. Popov, L. Henrard, and J. L. Sauvajol, Phys. Rev. B **75**, 155432 (2007).
[37] V. Derycke, R. Martel, J. Appenzeller, and Ph. Avouris, Appl. Phys. Lett. **80**, 2773 (2002).
[38] M. J. Biercuk, S. Ilani, C. M. Marcus, and P. L. McEuen, Top. Appl. Phys. **111**, 455 (2008).
[39] M. Lazzeri, C. Attaccalite, L. Wirtz, and F. Mauri, Phys. Rev. B **78**, 081406(R) (2008).
[40] P. J. Burke, IEEE Trans. NanoTechnol. **1**, 129 (2002).